Supporting Information

Superfine CoNi Alloy Embedded on Al_2O_3 Nanosheets for Efficient Tandem Catalytic Reduction of Nitroaromatic Compounds by Ammonia Borane

Sihang Cheng,[a] Yanchun Liu,[a] Yingnan Zhao,[a] Xinyu Zhao,[a] Zhongling Lang,*[a] Huaqiao Tan,*[a] Tianyu Qiu[a] and Yonghui Wang*[a]

Key Laboratory of Polyoxometalate Science of Ministry of Eduction, Faculty of Chemistry, Northeast Normal University, Changchun, 130024 (P.R. China)

**E-mail*: langzl554@nenu.edu.cn; tanhq870@nenu.edu.cn.; wangyh319@nenu.edu.cn.

Table of content

General procedure for the catalytic AB decomposition

In general, the catalyst (10 mg) was placed in a schlenk flask with 8 mL water, and placed in a water bath at 40 ± 1 ^{o}C. The hydrolysis reaction was started when 2 mL AB solution (0.6 M) was injected into the flask. Monitoring the volume variation of gas with a typical gas collection device until the gas ceases to bubble indicated completion of the reaction. For the durability test, after the AB decomposition was completed, the supernatant was removed via an external magnet, and then 10 mL of AB solution (0.12 M) was added while other conditions remained constant.

General procedure for the catalytic tandem reactions

Typically, nitroaromatic compounds (NACs, 0.1 mmol) and catalyst (3 mg) were charged into a glass vial with methanol (4 mL) and water (4 mL) at 323 K. The AB solution (0.4 mmol, 2 mL) was then injected into the vial. The conversion and selectivity of the target products were determined by GC-FID using n-dodecane as the internal standard. An external magnet was used to carry out a simple separation of the catalyst and the reaction liquid, and then a 10 ml mixed solution of NACs and AB (NACs/AB: 1/6, $V_{(H_2O)}/V_{(MeOH)}$: 2/3) was directly injected for the durability test of the tandem reaction.

Structural characterization

Powder X-ray diffraction (PXRD) measurements were carried through on a Rigaku D/max-IIB X-ray diffractometer with Cu-Kα radiation (λ = 1.5418 Å). Fourier transform infrared (FTIR) spectra were carried out on a Nicolet iS10 FTIR spectrometer. Transmission electron microscopy (TEM) and high-resolution TEM (HRTEM) images were carried out on JEOL-2100F and JEM-F 200 at an accelerating voltage of 200 kV. The morphology analysis was conducted on a field-emission scanning electron microscopy (FESEM; Hitachi SU-8010) at an accelerating voltage of 3 kV. The interrelated energy dispersive X-ray detector (EDX) spectra were carried out on a SU8000 ESEM FEG microscope. The nitrogen sorption measurement was carried through on an ASAP 2020 (Micromeritics, USA). The X-ray photoelectron spectroscopy (XPS) measurement were recorded on an ESCALAB 250 spectrometer (Thermo Electron Corp) with A1 Kα radiation (hv=1486.6 eV) as the excitation source. The contents of Co and Ni in Co_xNi_{1-x}/Al_2O_3 were quantified through a Teledyne Leeman Labs inductively coupled plasma atomic emission spectrometer (ICP-AES). The Brunauer-Emmett-Teller (BET) method was utilized to calculate the specific surface area by using adsorption data. The supernatant and gases generated by AB decomposition were separately detected utilizing a Shimadzu UV-2600 spectrophotometer (UV-Vis) and a gas chromatograph (Shimadzu, GC-2014C with a thermal conductivity detector). Hydrogen temperature programmed reduction (H_2-TPR) was conducted in a quartz tube reactor on a Micromeritics AutoChem II 2920 with a thermal conductivity detector (TCD). In each case, 50 mg of sample was sealed in the reactor, and then a gaseous mixture of H_2 and Ar (1:9, v/v) was fed to the reactor at 50 mL min^{-1}. The temperature was raised to 800 ^{o}C at a heating rate of 5 ^{o}C min^{-1}.

Catalytic performance of catalysts towards NH_3BH_3 decomposition

As illustrated in Fig. S12b, the decomposition rate of AB gradually augments with the increase concentration of catalysts $Co_{0.67}Ni_{0.33}/Al_2O_3$, presenting approximate first-order

reaction kinetics with respect to catalysts (inset of Fig. S12b). In contrast, since the rate of dehydrogenation much less relies on AB concentration, its linear fit slope of ln (rate) vs ln [AB] (inset of Fig. S12c) is about 0.148 closing to zero, which indicates that the reaction is pseudo zero-order reaction relative to the [AB]. These results are similar to that reported in the literatures.[1-3] Furthermore, the catalytic decomposition of AB at different temperatures has been also investigated. As shown in Fig. S12d, the AB decomposition rate is reduced with highly related to the decrease of temperature. At 298 K, the TOF value is about 34.54 min^{-1}. According to the *Arrhenius equation*, the activation energy (*Ea*) of $Co_{0.67}Ni_{0.33}/Al_2O_3$ is approximate 32.4 kJ/mol, which is obviously smaller than that of Co/Al_2O_3 (39.7 kJ/mol) and Ni/Al_2O_3 (37.5 kJ/mol), respectively, demonstrating the advantage of the optimized electronic structure of the bimetallic composition (Fig. S12d and Fig. S13). As shown in Table S2, the *Ea* value of this $Co_{0.67}Ni_{0.33}$ alloy is also lower than most of the reported non-noble metal catalysts.

In recycle experiments, owing to the good magnetism of CoNi alloy, the catalysts can be easily separated by a magnet. And then 10 mL of AB solution was quickly added for the next cycle. As illustrated in Fig. S12e, the catalytic activity of $Co_{0.67}Ni_{0.33}/Al_2O_3$ exhibits almost no decline in 12 runs, indicating the good stability and durability of the catalysts. The TEM and XRD of the recycled $Co_{0.67}Ni_{0.33}/Al_2O_3$ were displayed in Fig. S19a and Fig. S19b. It reveals the morphology and structure of $Co_{0.67}Ni_{0.33}/Al_2O_3$ have been well maintained. ICP-AES was further used to detect the loss of alloy catalysts in the catalysis. Negligible Co and Ni contents can be detected in the reaction supernatant, verifying the composition stability of the catalysts. This superior stability of $Co_{0.67}Ni_{0.33}/Al_2O_3$ for the catalytic decomposition of AB might be related to the fact that CoNi alloys are firmly embedded in the alumina sheets, which prevents their aggregation, leaching and oxidation during catalytic decomposition effectively.

Computational details

All periodic calculations in this work were performed by means of spin-polarized density functional theory (DFT) methods with the PBE functional that implemented in Vienna ab ignition simulation package (VASP 5.4).[22,23] A suitable k-point grid of 3×3×1 was generated with Monkhorst-Pack algorithm.[24] The kinetic energy cut off was set to 400 eV. All results were obtained until the forces and energy reach to smaller than 0.05 eV $Å^{-1}$ and 10^{-5} eV respectively. The kinetic barrier for RDS was explored by combining the climbing-image nudged-elastic-band (CI-NEB) algorithm and improved dimer methods. And the transition state was confirmed as only one imaginary frequency along the reaction coordinate by frequency analysis.

We have constructed three correlative theoretical models to simulate their activity toward AB hydrolysis and nitrobenzene reduction. The parent Ni (111) and Co (111) surfaces were simulated by a 4×4 supercell with three layers. Due to the well lattice match between Ni (a = b = c = 3.524 Å) and Co (a = b = c = 3.544 Å), the Co_2Ni (111) surface was modeled by substituting 1/3 of Co atoms with Ni based on Co(111). A vacuum larger than 15 Å perpendiculars to the surface avoided the interaction between repeated cells. The bottom two metal layers were frozen during the optimization.

Fig. S1 The colors of the as-synthesized $Co_xNi_{1-x}Al$-LDH: A-CoAl-LDH, B-$Co_{0.83}Ni_{0.17}Al$-LDH, C-$Co_{0.67}Ni_{0.33}Al$-LDH, D-$Co_{0.50}Ni_{0.50}Al$-LDH, E-$Co_{0.33}Ni_{0.67}Al$-LDH, F-NiAl-LDH.

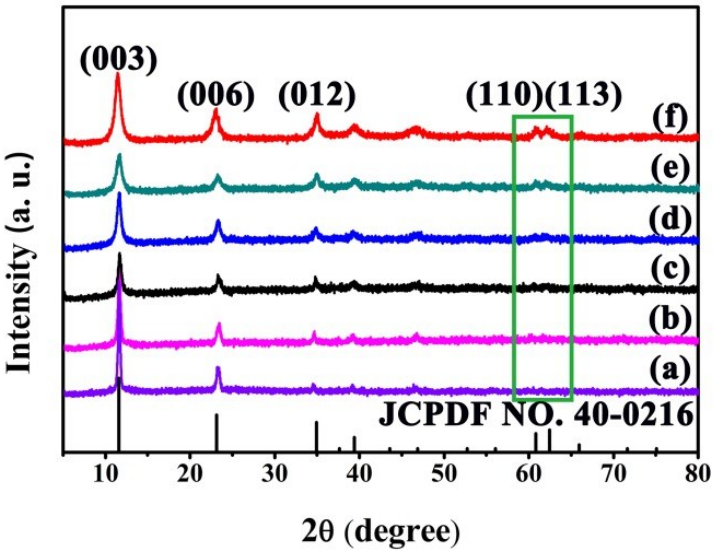

Fig. S2 XRD patterns of $Co_xNi_{1-x}Al$-LDH precursors: (a-Violet) CoAl-LDH, (b-Magenta) $Co_{0.83}Ni_{0.17}Al$-LDH, (c-Black) $Co_{0.67}Ni_{0.33}Al$-LDH, (d-Blue) $Co_{0.50}Ni_{0.50}Al$-LDH, (e-Dark Cyan) $Co_{0.33}Ni_{0.67}Al$-LDH, (f-Red) NiAl-LDH.

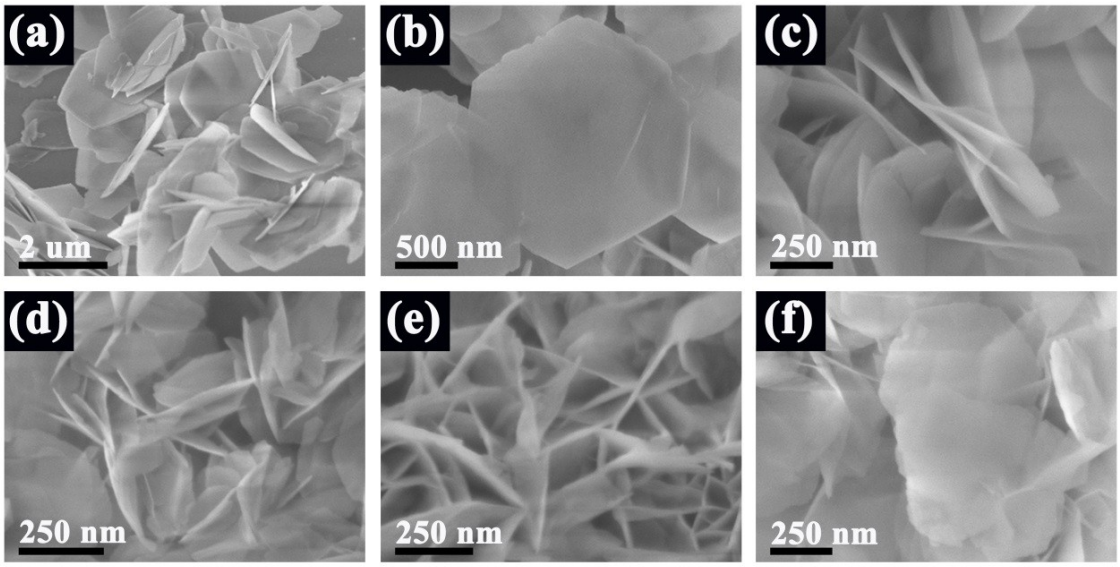

Fig. S3 SEM patterns of $Co_xNi_{1-x}Al$-LDH precursors: (a) CoAl-LDH, (b) $Co_{0.83}Ni_{0.17}Al$-LDH, (c) $Co_{0.67}Ni_{0.33}Al$-LDH, (d) $Co_{0.5}Ni_{0.5}Al$-LDH, (e) $Co_{0.33}Ni_{0.67}Al$-LDH, (f) NiAl-LDH. The thickness of the nanosheets is approximately 35, 15, 6, 5.8, 5.28, 4.5 nm, respectively.

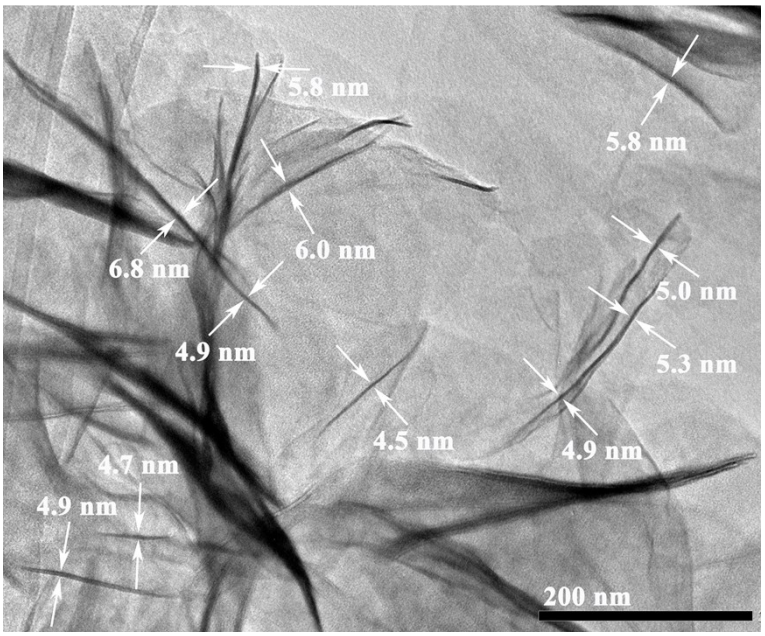

Fig. S4 TEM image of $Co_{0.67}Ni_{0.33}Al$-LDH.

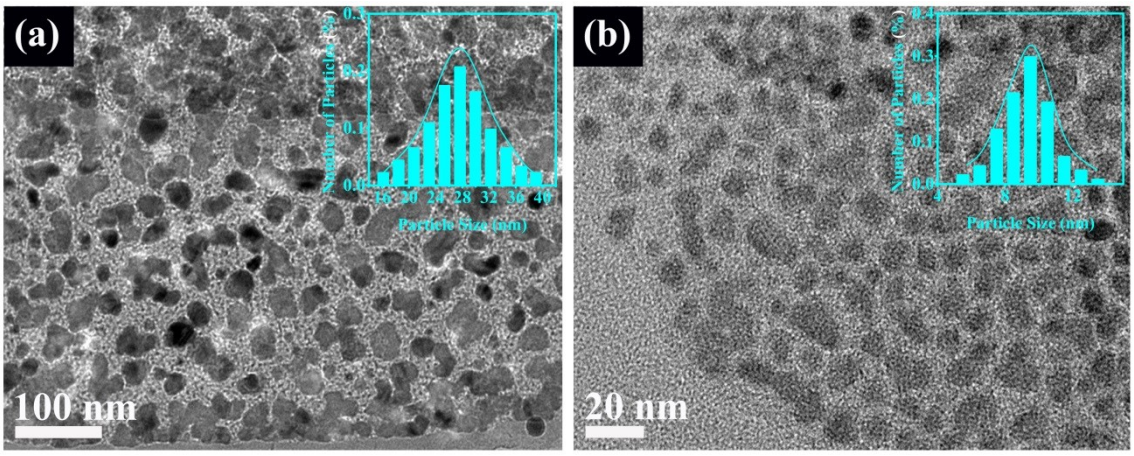

Fig. S5 TEM images of (a) Co/Al_2O_3 and (b) Ni/Al_2O_3 (the inset is the particle size distribution).

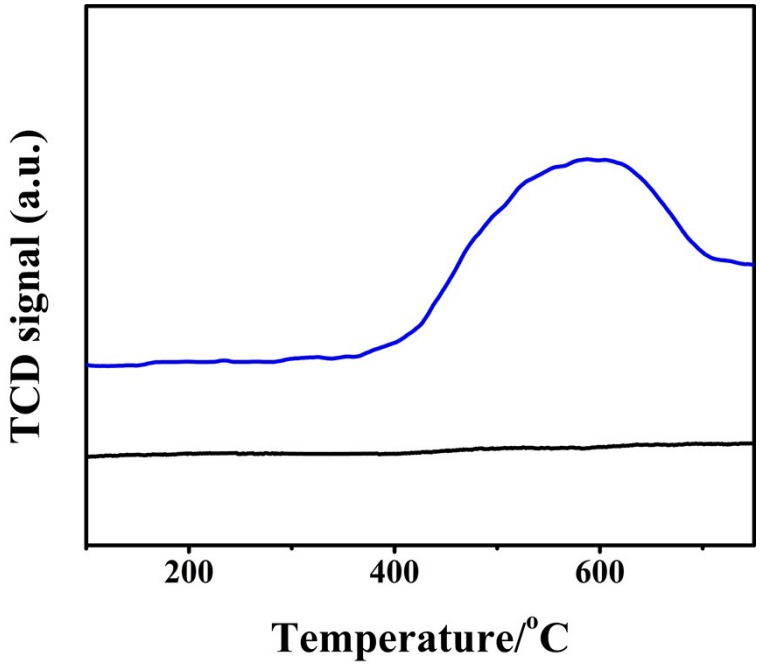

Fig. S6 H_2-TPR profiles of (blue) $Co_{0.67}Ni_{0.33}Al$-LDH and (black) as-prepared $Al(OH)_X$. The broad peak at 600 °C is attributed to the reduction of Co^{2+} and Ni^{2+}. No peaks were observed in the TPR of the as-prepared $Al(OH)_X$ sample, indicating that it could not be reduced at 650 °C under H_2 atmosphere.

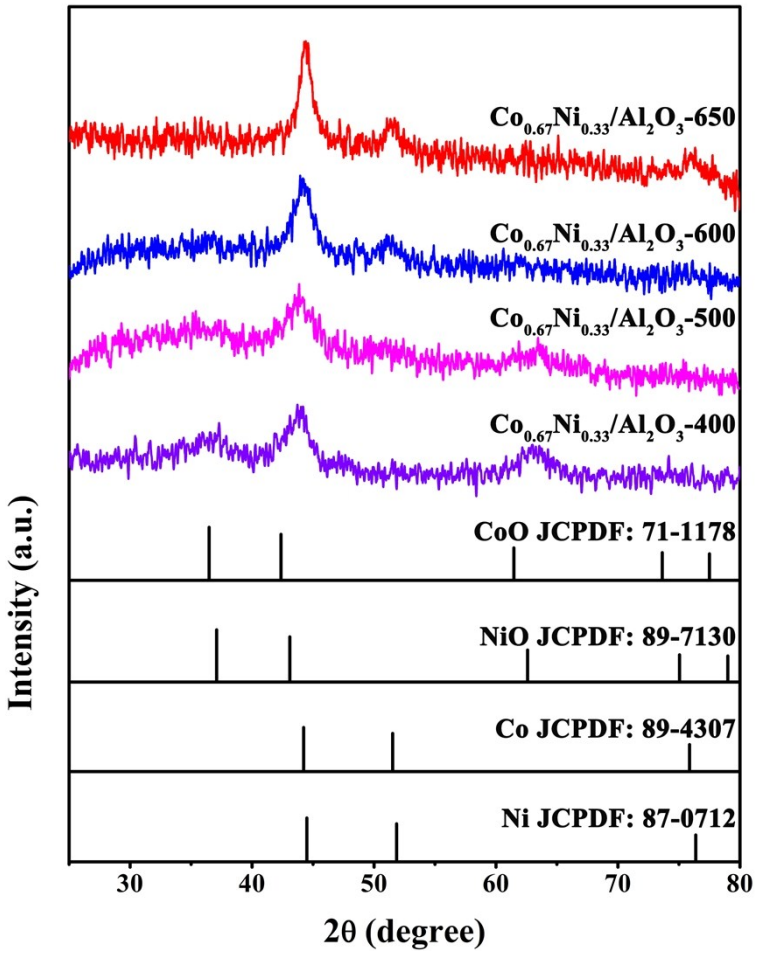

Fig. S7 XRD patterns for $Co_{0.67}Ni_{0.33}/Al_2O_3$-*x* (*x* = reduction temperature). The XRD patterns of $Co_{0.67}Ni_{0.33}/Al_2O_3$-x with different reduction temperatures are consistent with the TPR result, which demonstrate that cobalt and nickel can be reduced successfully at H_2/Ar atmosphere at 650 °C.

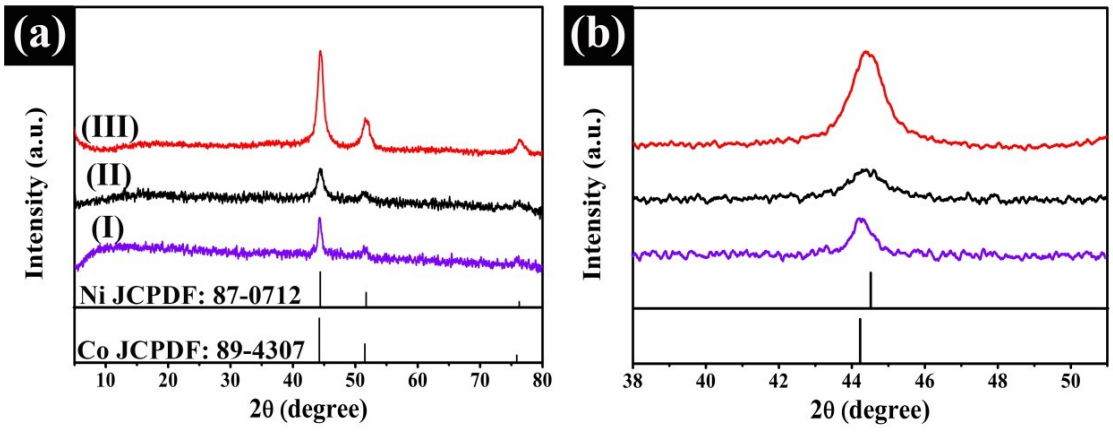

Fig. S8 (a) XRD patterns of: (I) Co/Al_2O_3, (II) $Co_{0.67}Ni_{0.33}/Al_2O_3$, (III) Ni/Al_2O_3. (b) Amplified part of the XRD patterns of (a).

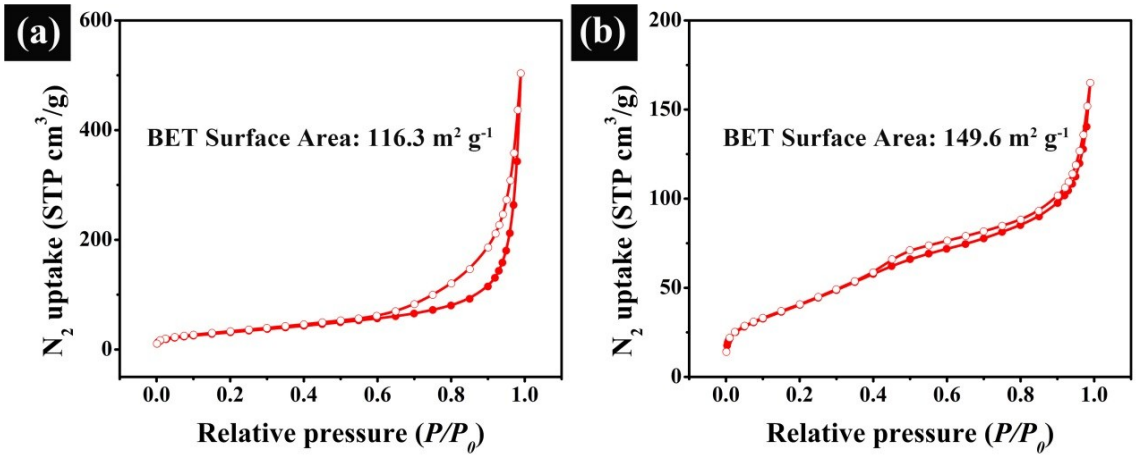

Fig. S9 The N_2 adsorption isotherms of (a) Co/Al_2O_3 and (b) Ni/Al_2O_3 catalysts indicated BET surface areas of 116.3 and 149.6 $m^2 \cdot g^{-1}$, respectively. (Filled and open symbols represent adsorption and desorption branches, respectively)

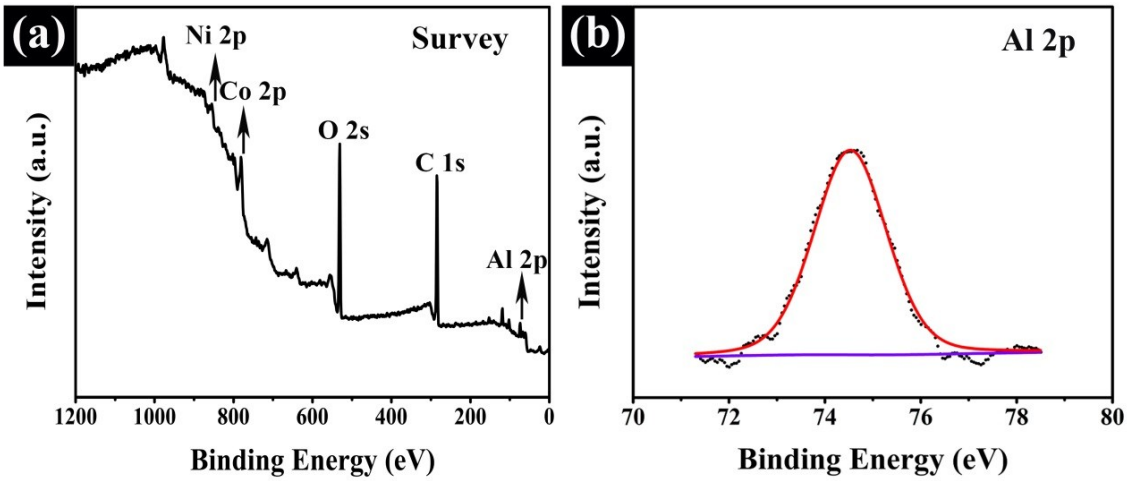

Fig. S10 XPS spectra of $Co_{0.67}Ni_{0.33}/Al_2O_3$: (a) survey and (b) Al.

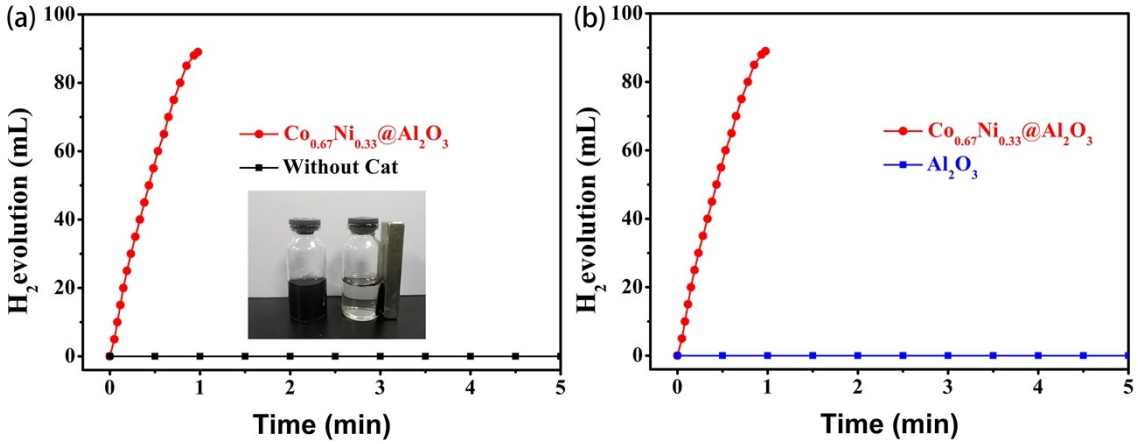

Fig. S11 Control experiments of AB decomposition (a) and (b): red represents $Co_{0.67}Ni_{0.33}/Al_2O_3$; black represents without catalyst and blue represents as-prepared Al_2O_3 catalyst. The inset is the magnetic separation after $Co_{0.67}Ni_{0.33}/Al_2O_3$ catalytic decomposition of AB.

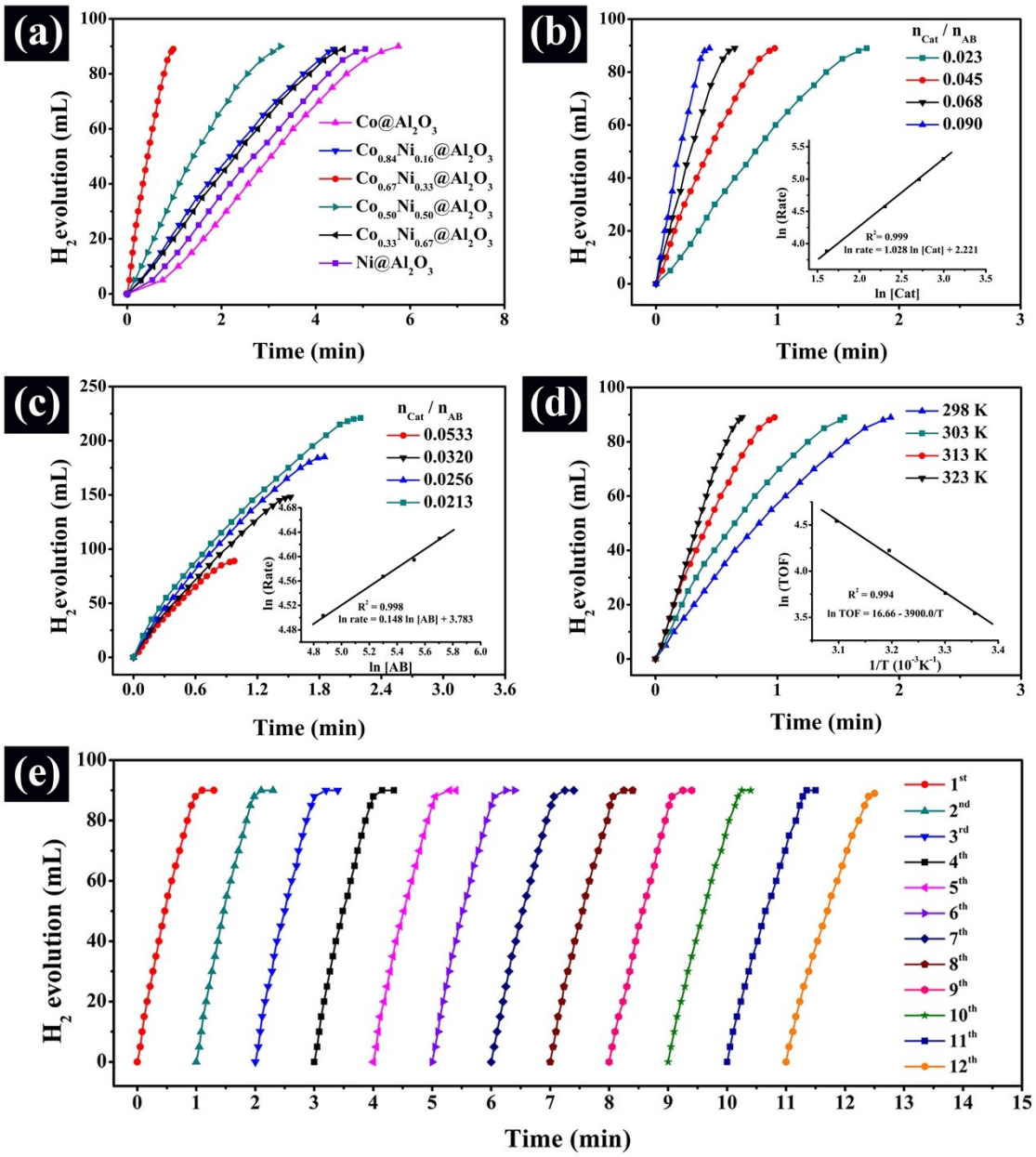

Fig. S12 (a) Stoichiometric hydrogen evolution from AB (0.12 M, 10 ml) hydrolysis catalyzed by a series of Co_xNi_{1-x}/Al_2O_3 catalysts at 313 K. (b-c) The relationship between the H_2 generation rate vs the (b) [$Co_{0.67}Ni_{0.33}/Al_2O_3$] and the (c) [AB]. (d) $Co_{0.67}Ni_{0.33}/Al_2O_3$ catalyzed AB decomposed at 298-313 K (e) Recycles of the decomposition of AB: $Co_{0.67}Ni_{0.33}/Al_2O_3$ (10 mg), AB (0.12 M, 10.0 mL), 313 K. (Insets b and c: the logarithmic plots of H_2 generation rate vs. the concentration of $Co_{0.67}Ni_{0.33}/Al_2O_3$ and AB, respectively. Inset d: the corresponding Arrhenius plots of ln TOF vs. 1/T.)

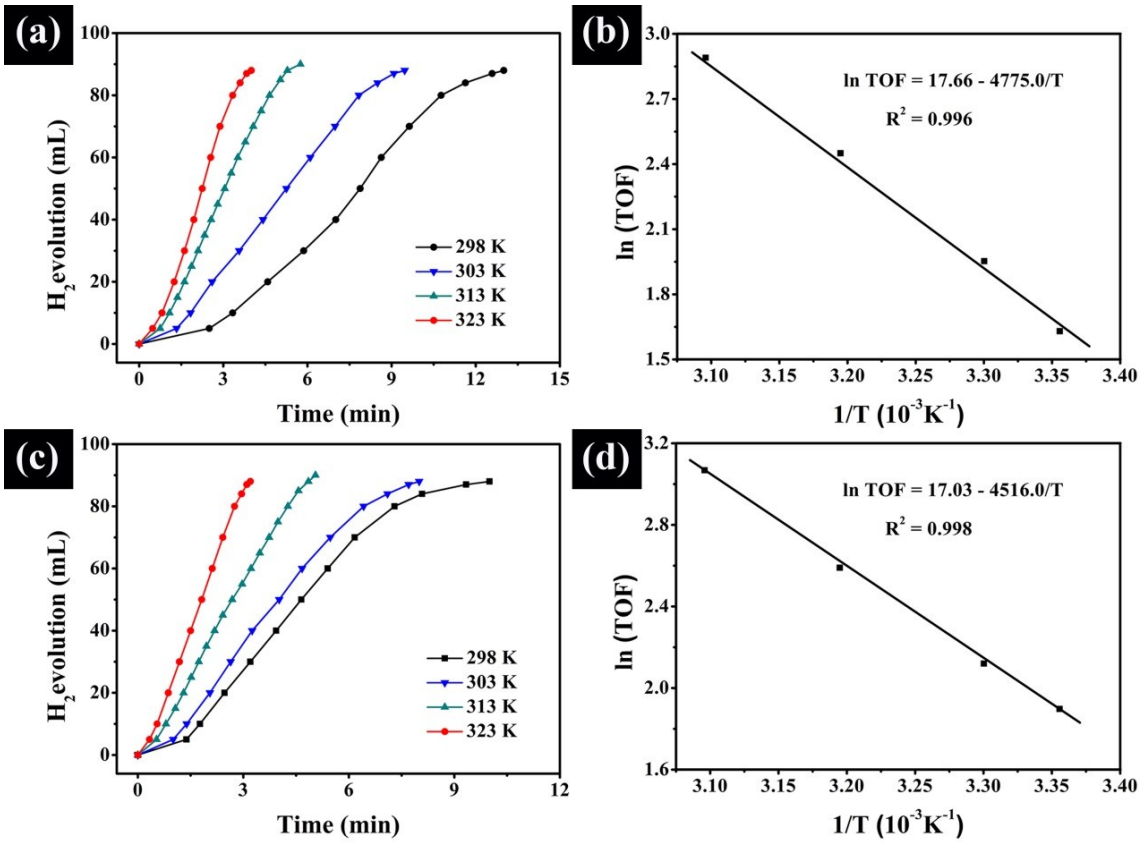

Fig. S13 (a) and (c): The Volume of H_2 production vs. time from the decomposition of AB catalyzed by Co/Al_2O_3 and Ni/Al_2O_3. (b) and (d) correspond to Arrhenius plot of ln (TOF) versus 1/T, respectively.

NMR S1. p-Methoxyaniline

^{1}H-NMR (500 MHz, d6-DMSO): 6.64 (m, 2H), 6.52 (m, 2H), 4.57 (s, 2H), 3.61 (s, 3H). ^{13}C-NMR (125 MHz, d6-DMSO): 151.12, 142.78, 115.40, 114.95, 55.74.

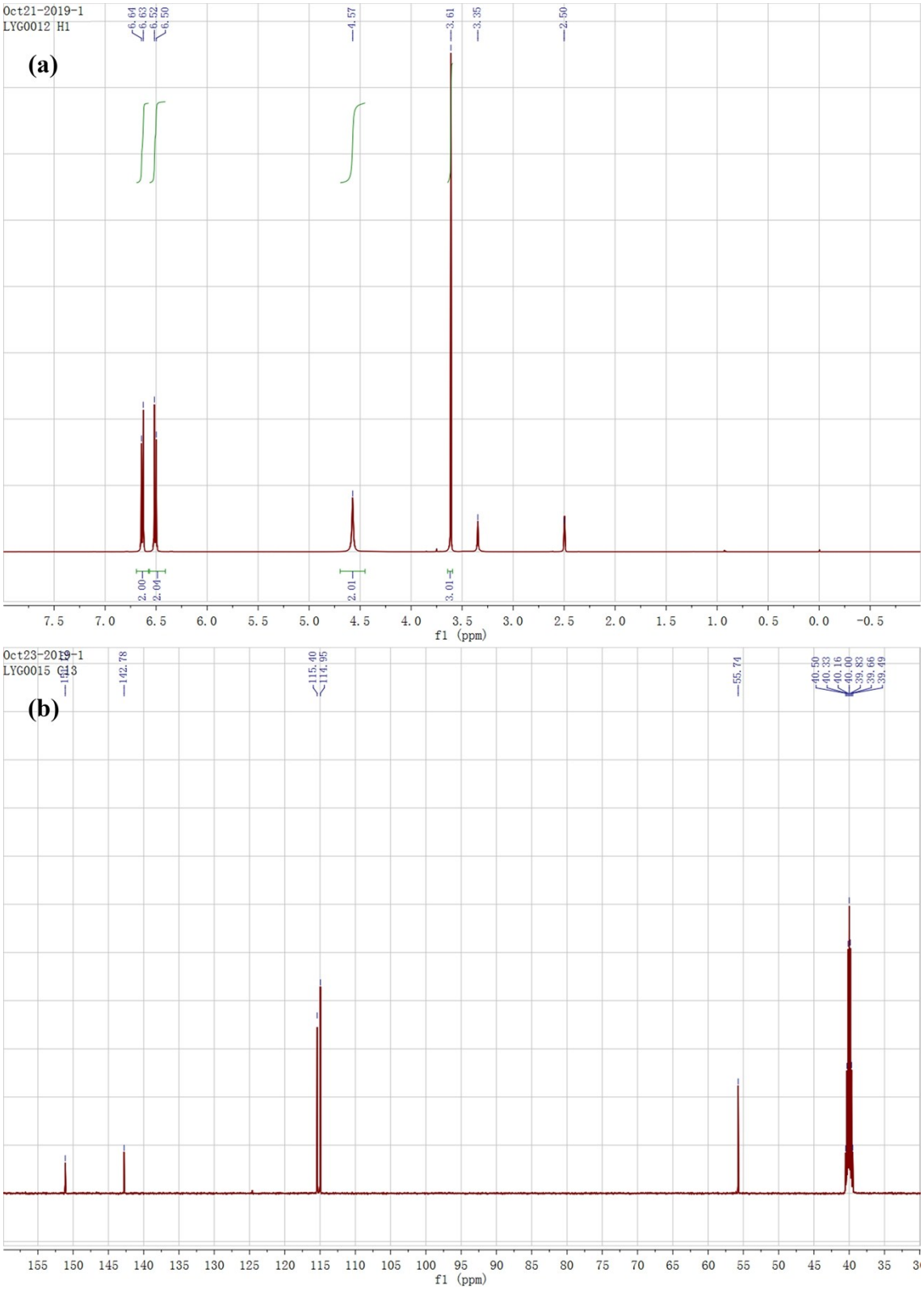

Fig. S14 ^{1}H NMR (a) and ^{13}C NMR (b) spectrums of the corresponding target product amine after the tandem hydrogenation of 4-methoxynitrobenzene.

NMR S2. Aniline

^{1}H-NMR (500 MHz, d6-DMSO): 7.00 (t, 2H), 6.56 (m, 2H), 6.48 (t, 1H), 4.97 (s, 2H). ^{13}C-NMR (125 MHz, d6-DMSO): 149.57, 129.58, 103.52, 100.43.

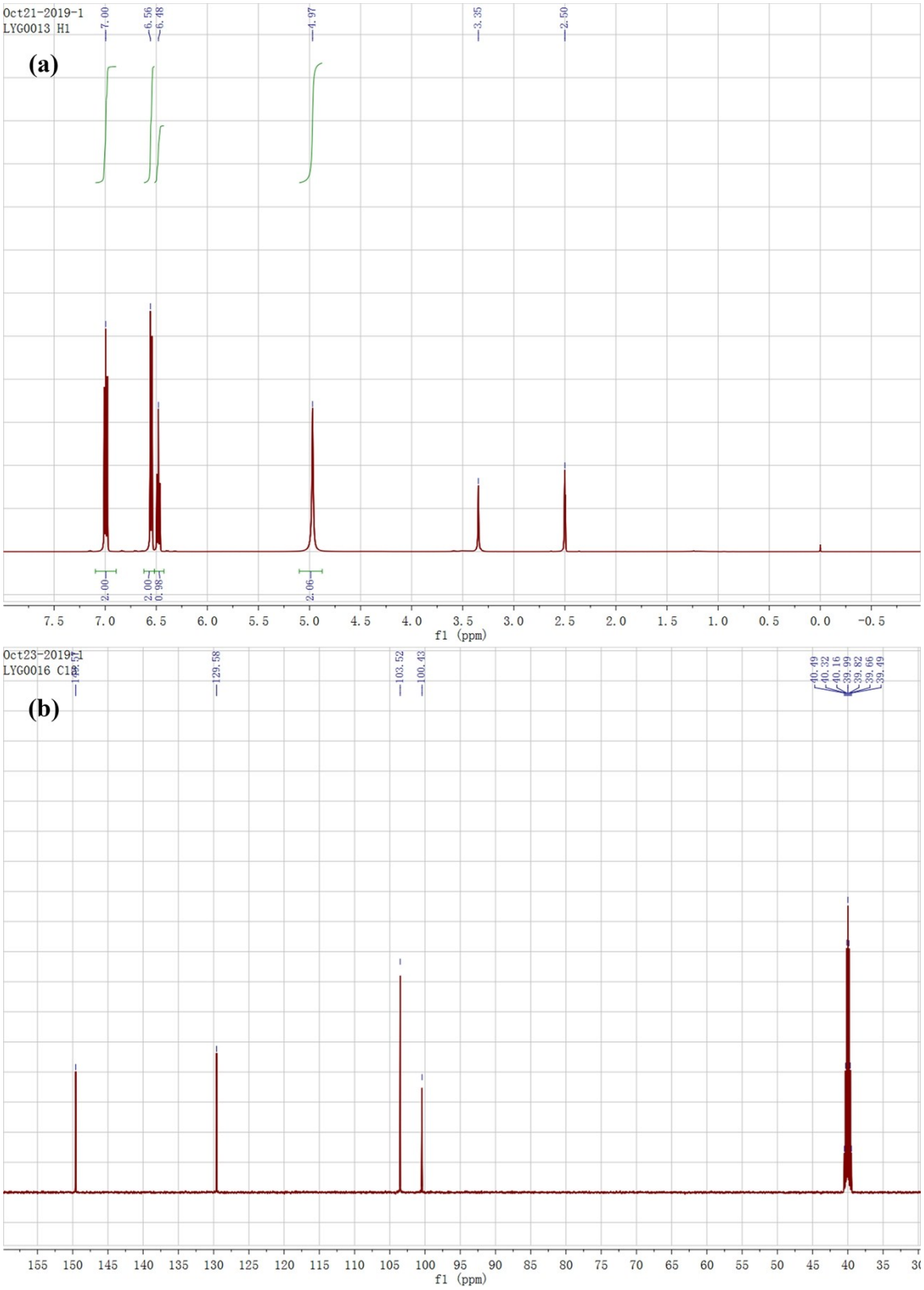

Fig. S15 ^{1}H NMR (a) and ^{13}C NMR (b) spectrums of the corresponding target product amine after the tandem hydrogenation of nitrobenzene.

NMR S3. m-Phenylenediamine

^{1}H-NMR (500 MHz, d6-DMSO): 6.65 (t, 2H), 5.81 (t, 1H), 5.79 (dd, 2H), 4.63 (s, 4H). ^{13}C-NMR (125 MHz, d6-DMSO): 149.07, 129.26, 116.08, 114.32.

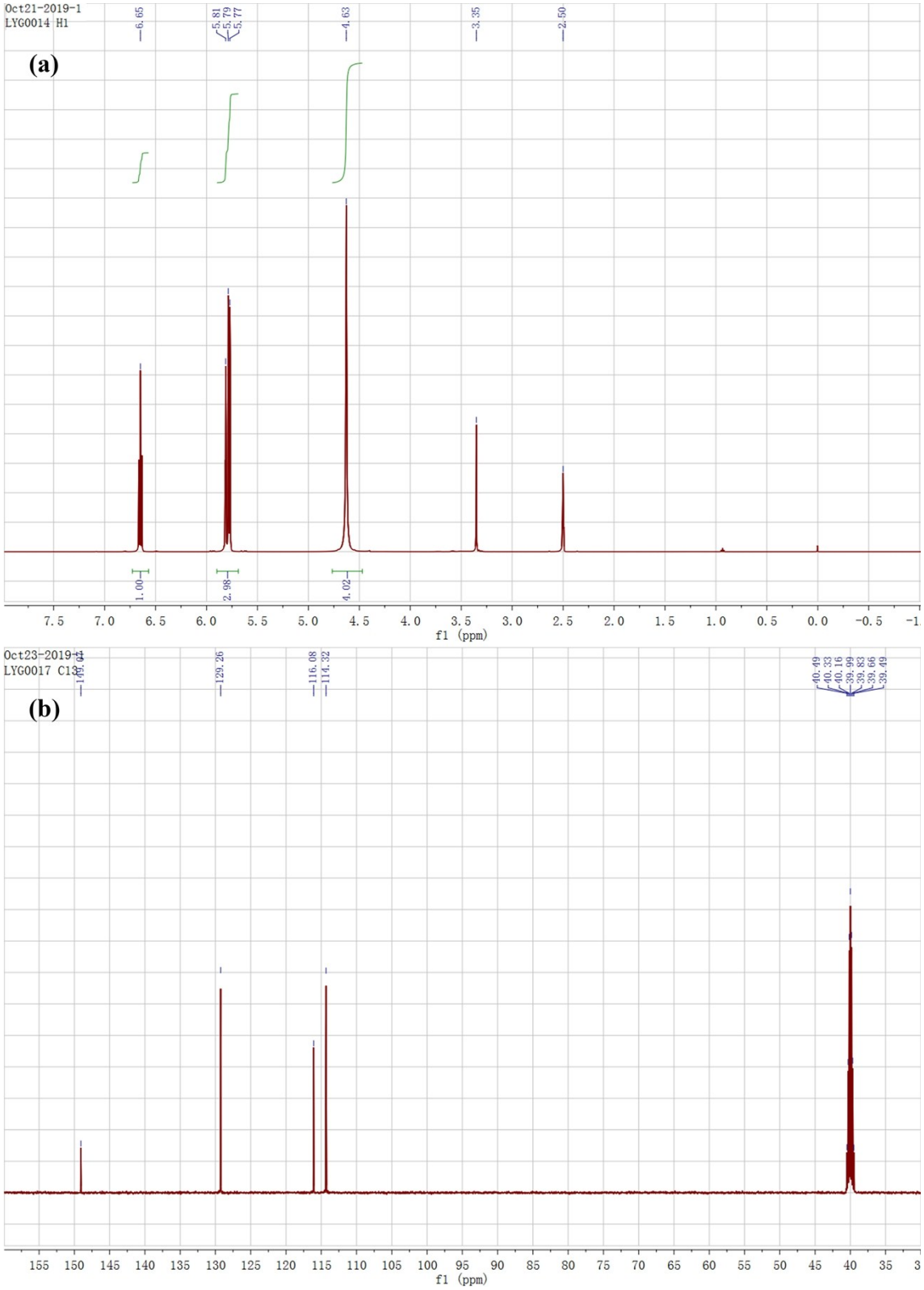

Fig. S16 ^{1}H NMR (a) and ^{13}C NMR (b) spectrums of the corresponding target product amine after the tandem hydrogenation of 1, 3-dinitrobenzene.

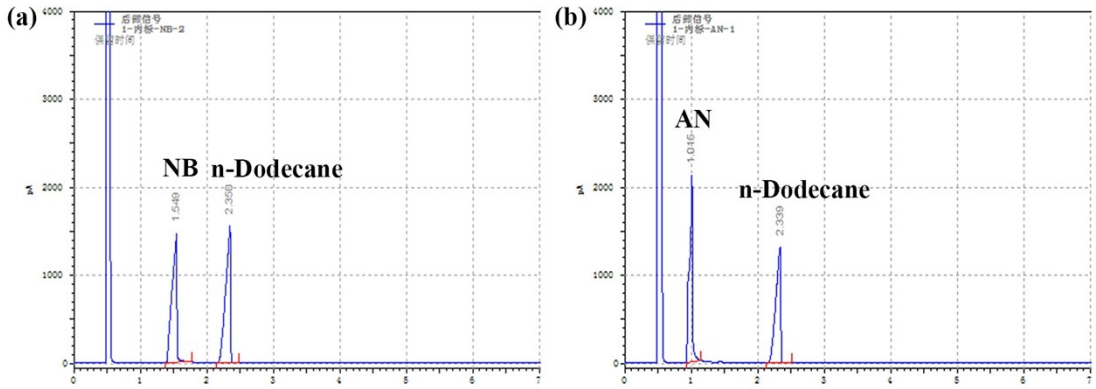

Fig. S17 The spectrums of (a) nitrobenzene and (b) the corresponding product were determined by gas chromatography internal standard method (nitrobenzene: NB; aniline: AN; n-dodecane is the internal standard).

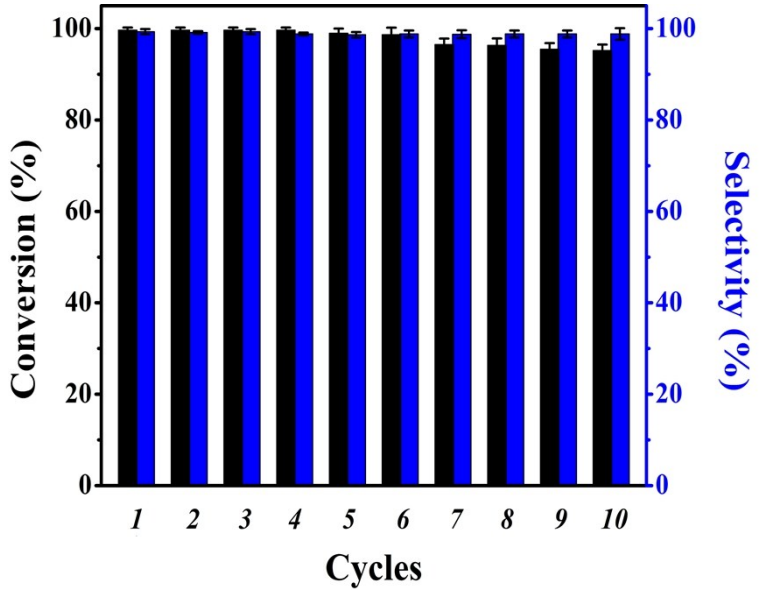

Fig. S18 Recycling test of hydrogenation of 4-methoxynitrobenzene to the corresponding amine by $Co_{0.67}Ni_{0.33}/Al_2O_3$ catalyst at 323 K (4-methoxynitrobenzene = 0.1 mmol, cat = 3 mg, AB = 0.6 mmol, T = 323 K).

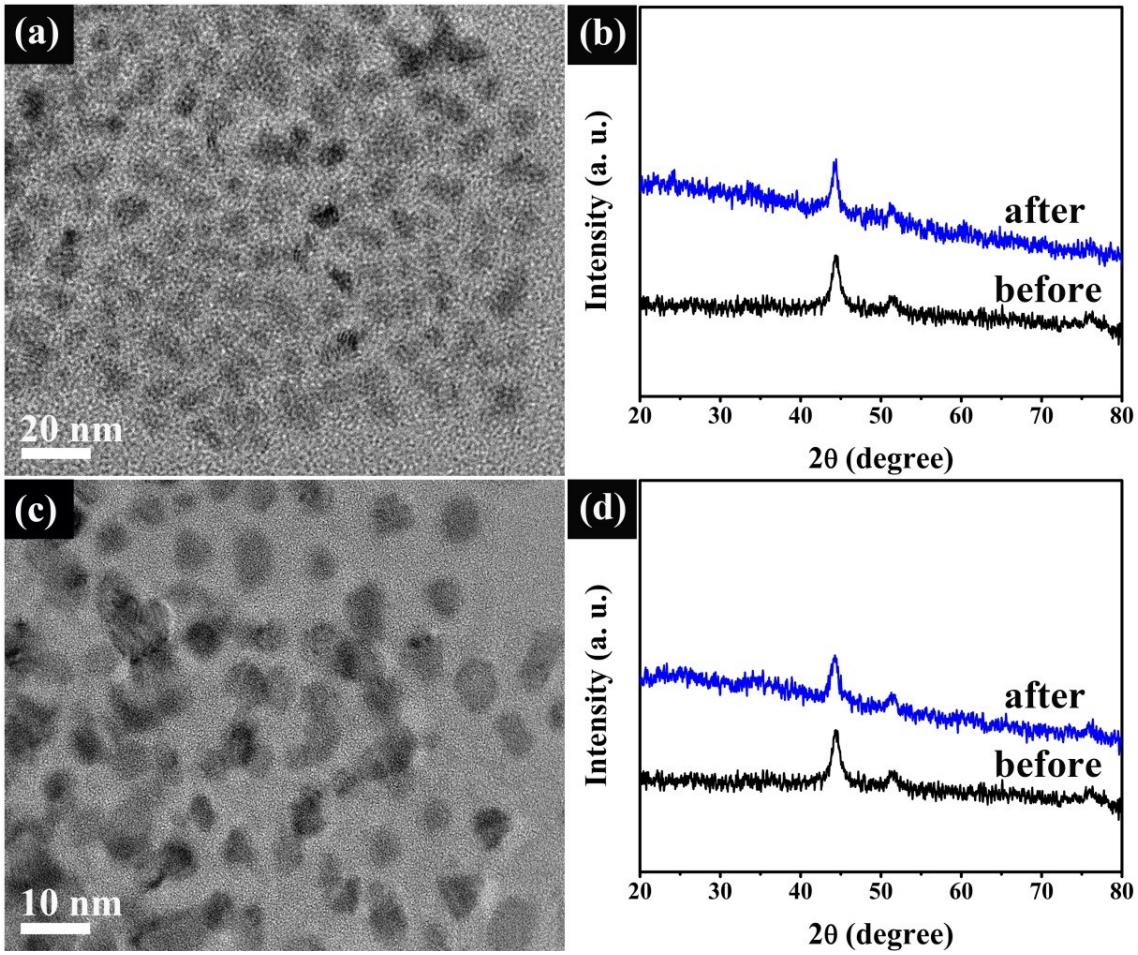

Fig. S19 (a) TEM and (b) XRD images of $Co_{0.67}Ni_{0.33}/Al_2O_3$ catalyst after 12 cycles of AB decomposition at 313 K. (c) TEM and (d) XRD images of the $Co_{0.67}Ni_{0.33}/Al_2O_3$ catalyst after 10 cycles of hydrogenation of 4-methoxynitrobenzene to the corresponding amine at 323 K.

Table S1 The ratios of Co and Ni in various Co_xNi_{1-x}/Al_2O_3 nanocatalysts.

Samples	Added value of Co:Ni	EDX-Measured Co:Ni	ICP-AES-Measured Co:Ni
Co/Al_2O_3	1:0	1:0	1:0
$Co_{0.83}Ni_{0.17}/Al_2O_3$	0.83:0.17	0.82:0.18	0.825:0.175
$Co_{0.67}Ni_{0.33}/Al_2O_3$	0.67:0.33	0.66:0.34	0.668:0.332
$Co_{0.50}Ni_{0.50}/Al_2O_3$	0.50:0.50	0.50:0.50	0.497:0.503
$Co_{0.33}Ni_{0.67}/Al_2O_3$	0.33:0.67	0.32:0.68	0.326:0.674
Ni/Al_2O_3	0:1	0:1	0:1

Table S2 The values of activation energy (Ea) for hydrogen evolution from the decomposition of AB catalyzed by different catalysts.

Catalyst	Ea (kJ mol^{-1})	TOF (min^{-1})	Ref.
$Ni_{30}Pd_{70}$/rGO	45.0	28.7	[4]
$Ni_{0.74}Ru_{0.26}$ alloy	37.2	—	[5]
AuCo/NXC-1	31.9	42.1	[6]
$Cu_{0.2}Co_{0.8}$/PDA-rGO	54.9	55.6[b]	[7]
NiCo alloy	49.4	4.3[d]	[8]
$Cu_{0.8}Co_{0.2}O$-GO	45.5	70.0	[9]
$Ni_{0.7}Co_{1.3}P$	43.2	58.4[a]	[10]
$Cu_{0.5}Ni_{0.5}$/CMK-1	43.0	54.8	[11]
CuNi/MCM-41	38.0	10.7	[12]
$Co_{0.67}Ni_{0.33}/Al_2O_3$	32.4	34.5	This work
$Ni_{0.9}Mo_{0.1}$/grapheme	21.8	66.7	[13]
CoNi/Graphene	13.5	16.8	[14]
$Cu_{0.72}Co_{0.18}Mo_{0.1}$ NPs	45.0	46.0	[15]
Cu@FeCo NPs	38.75	10.5	[16]
Ni NPs/ZIF-8	42.7	35.3	[17]
Co/NPCNW	7.3	25.4	[18]
Ni@MSC-30	—	30.7	[19]
Ni/C	28 ± 2	8.8	[20]
Co/γ-Al_2O_3	62	2.08	[21]
Ni/γ-Al_2O_3	—	2.5[c]	[21]

Table S3 as-prepared Al_2O_3 catalyzed tandem reaction of various R-NO_2 compounds[a]

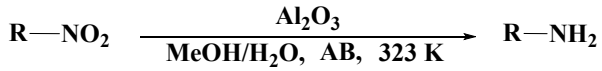

Entry	Substrate	Product	Yield (%)	Time
1	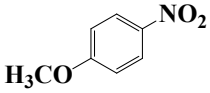	—	—	9 h
2	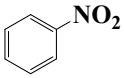	—	—	9 h
3[b]	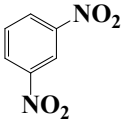	—	—	9 h

[a]General reaction conditions: 0.1 mmol nitroarene, 0.4 mmol NH_3BH_3, 3 mg $Co_{0.67}Ni_{0.33}/Al_2O_3$ (32%, 0.0163 mmol cat), 10 mL of methanol/water (v/v = 2/3), 323 K; [b]0.6 mmol NH_3BH_3.

Table S4 $Co_{0.67}Ni_{0.33}/Al_2O_3$-catalyzed tandem reaction of various R-NO_2 compounds[a]

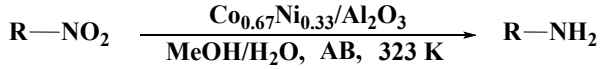

Entry	Substrate	Product	Yield (%)	Time
1[b]	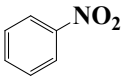	—	—	9 h
2[c]	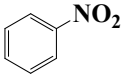	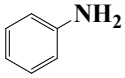	~ 6	9 h
3	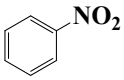	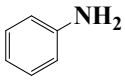	> 99	15 min
4[d]	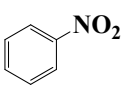	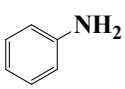	> 94	50 min
5[e]	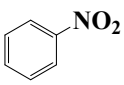	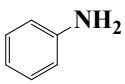	> 99	40 min
6[f]	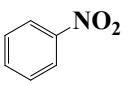	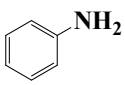	> 99	40 min

[a]General reaction conditions: 0.1 mmol nitroarene, 0.4 mmol NH_3BH_3, 3 mg $Co_{0.67}Ni_{0.33}/Al_2O_3$ (32%, 0.0163 mmol cat), 10 mL of methanol/water (v/v = 2/3), 323 K; [b]Without any catalysts; [c]NH_3BH_3 was replaced by 1 bar hydrogen.[d]$Co_{0.67}Ni_{0.33}/Al_2O_3$ catalyst was replaced by 3 mg Co/Al_2O_3. [e]$Co_{0.67}Ni_{0.33}/Al_2O_3$ catalyst was replaced by 3 mg Ni/Al_2O_3. [f]NB can also be well reduction by $Co_{0.67}Ni_{0.33}/Al_2O_3$ catalyst at 25 °C.

Table S5 The adsorption energy (eV) for each intermediate adsorbed on Ni(111), Co_2Ni(111)and Co(111).

E_{ads} (eV)	Ni(111)	Co_2Ni(111)	Co(111)
H_2O-$NH_3BH_3^*$	-0.95	-1.23	-1.30
H^*	-0.67	-0.43	-0.53
Ph-NO_2^*	-1.63	-0.78	-0.83
Ph-NO^*	-2.93	-1.77	-1.64
Ph-$NHOH^*$	-1.75	-1.04	-1.18
Ph-NH_2^*	-1.57	-0.75	-0.85

Reference

1. C. C. Hou, Q. Li, C. J. Wang, C. Y. Peng, Q. Q. Chen, H. F. Ye, W. F. Fu, C. M. Che, N. López and Y. Chen, Energy. Environ. Sci., 2017, 10, 1770-1776.
2. J. K. Zhang, W. Y. Chen, H. B. Ge, C. Q. Chen, W. J. Yan, Z. Gao, J. Gan, B. Y. Zhang, X. Z. Duan and Y. Qin, Appl. Catal., B, 2018, 235, 256-263.
3. L. Zhang, Y. Y. Wang, J. L. Li, X. Y. Ren, H. Lv, X. S. Su, Y. C. Hu, D. D. Xu and B. Liu, ChemCatChem, 2018, 10, 4910-4916.
4. N. S. Çiftci and Ö. Metin, *Int. J. Hydrogen Energy*, 2014, 39, 18863-18870.
5. G. Z. Chen, S. Desinan, R. Rosei, F. Rosei and D. L. Ma, *Chemistry*, 2012, 18, 7925-7930.
6. L. L. Guo, X. J. Gu, K. Kang, Y. Y. Wu, J. Cheng, P. L. Liu, T. S. Wang and H. Q. Su, *J. Mater. Chem. A*, 2015, 3, 22807-22815.
7. F. Z. Song, Q. L. Zhu, X. C. Yang and Q. Xu, *Chemnanomat*, 2016, 2, 942-945.
8. S. Q. Zhou, M. Wen, N. Wang, Q. S. Wu, Q. N. Wu and L. Y. Cheng, *J. Mater. Chem.*, 2012, 22, 16858-16864.
9. K. Feng, J. Zhong, B. H. Zhao, H. Zhang, L. Xu, X. H. Sun and S. T. Lee, *Angew. Chem.*, *Int. Ed.,* 2016, 128, 12129-12133.
10. C. C. Hou, Q. Li, C. J. Wang, C. Y. Peng, Q. Q. Chen, H. F. Ye, W. F. Fu, C. M. Che, N. López and Y. Chen, *Energy. Environ. Sci.,* 2017, 10, 1770-1776.
11. H. Yen, Y. Seo, S. Kaliaguine and F. Kleitz, *ACS Catal.,* 2015, 5, 5505-5511.
12. Z. H. Lu, J. P. Li, G. Feng, Q. L. Yao, F. Zhang, R. Y. Zhou, D. J. Tao, X. S. Chen and Z. Q. Yu, *Int. J. Hydrogen Energy*, 2014, 39, 13389-13395.
13. Q. L. Yao, Z. H. Lu, W. Huang, X. S. Chen and J. Zhu, *J. Mater. Chem. A*, 2016, 4, 8579-8583.
14. W. Q. Feng, L. Yang, N. Cao, C. Du, H. M. Dai, W. Luo and G. Z. Cheng, *Int. J. Hydrogen Energy*, 2014, 39, 3371-3380.
15. Q. L. Yao, K. Yang, X. L. Hong, X. S. Chen and Z. H. Lu, *Catal. Sci. Technol.*, 2018, 8, 870-877.
16. F. Y. Qiu, Y. L. Dai, L. Li, C. C. Xu, Y. A. Huang, C. C. Chen, Y. J. Wang, L. F. Jiao and H. T. Yuan, *Int. J. Hydrogen Energy*, 2014, 39, 436-441.
17. C. Wang, J. Tuninetti, Z. Wang, C. Zhang, R. Ciganda, L. Salmon, S. Moya, J. Ruiz and D. Astruc, *J. Am. Chem. Soc.*, 2017, 139, 11610-11615.
18. L. M. Zhou, J. Meng, P. Li, Z. L. Tao, L. Q. Mai and J. Chen, *Mater. Horiz.*, 2017, 4, 268-273.
19. P. Z. Li, A. Aijaz and Q. Xu, *Angew. Chem.*, *Int. Ed.,* 2012, 51, 6753-6756.
20. O. Metin, V. Mazumder, S. Ozkar and S. Sun, *J. Am. Chem. Soc.*, 2010, 132, 1468-1469.
21. Q. Xu and M. Chandra, *J. Power Sources*, 2006, 163, 364-370.
22. J. P. Perdew, K. Burke, M. Ernzerhof, *Phys. Rev. Lett.,* 1997, 78, 1396.
23. G. Kresse, J. Furthmüller, Comput. *Mater. Sci.,* 1996, 6, 15.
24. H. J. Monkhorst, J. D. Pack, Phys. *Rev. B: Solid State,* 1976, 13, 5188.